Chemical Interpretation of Charged Point Defects in Semiconductors: A Case Study of Mg_2Si

Michael Y. Toriyama,[a*] Madison K. Brod,[a] and G. Jeffrey Snyder[a*]

The number of excess charge carriers generated by a point defect, defined by the "charge state" of a defect, is oftentimes an important quantity used to engineer the electronic properties of semiconductors. Here, we develop a molecular orbital theory-based framework for interpreting the charge state(s) of a point defect, which is based on local chemical interactions between the defect and the atoms surrounding the defect site. We demonstrate how the framework can be applied to native defects in Mg_2Si, such as interstitials, vacancies, and antisite defects, by utilizing symmetry principles and Density Functional Theory calculations. We anticipate that such an interpretive framework will guide efforts to engineer electronic and optical properties of semiconductors through manipulation of intrinsic and extrinsic defects.

1 Introduction

Point defects are used to control a variety of electronic and optical properties of materials, in which the concept of a *charge state* of a defect is oftentimes useful. The charge state of a defect is the relative charge that is localized at the defect site. Analogous to Kröger-Vink notation,[1] we say that the defect has a negative charge state when additional electrons are localized at the defect site (i.e., an acceptor), a positive charge state when electrons are delocalized from the defect site (i.e., a donor), and a neutral 0 charge state otherwise. In phosphorus-doped silicon for example, it is typically understood that a P dopant (5 valence e^-) donates an electron to the electron reservoir when substituting for Si (4 valence e^-). Since an electron delocalizes from the P dopant in this scenario, we label the defect with a $+1$ charge state, denoted by a superscript as P_{Si}^{+1}.

Although the charge state of P_{Si} could be understood simply from valence electron counting, this is not true in general since the placement of the excess charge (either near the defect site or in the electron reservoir) depends on the energy of the electron reservoir (i.e., the Fermi level E_F).[2] In fact, a point defect may possess multiple charge states depending on the position of E_F. A famous example of this is the oxygen vacancy (V_O) in ZnO, where computational studies[3–10] and EPR experiments[11] have asserted that the charge state is neutral (i.e., V_O^0) when E_F is near the conduction band minimum, and the charge state is $+2$ (i.e. V_O^{+2}) when E_F is near the valence band maximum.

The charge state(s) of a point defect can be understood from the exchanging of electrons between the defective region and an electron reservoir.[2,12] For a hypothetical II-VI compound AB as illustrated in Figure 1, the creation of a B vacancy (V_B) for example leaves 2 electrons remaining, since B has 6 valence electrons. The charge state of V_B is determined by whether the remaining 2 electrons are released to the electron reservoir, which we can understand using a Le Chatelier's Principle-like argument. If E_F is close to the conduction band (Figure 1a), then the 2 electrons will likely remain localized at the defect site (V_B^0) due to the heavily populated electron reservoir, similar to how a chemical reaction

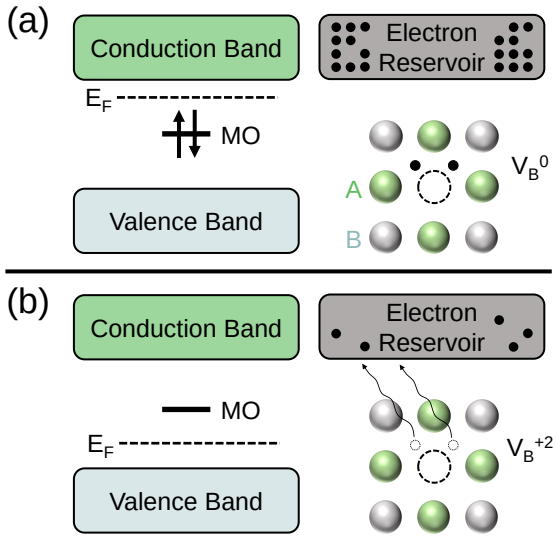

Fig. 1 Illustrations of the 0 and +2 charge states of the anion vacancy (V_B) in a hypothetical II-VI compound AB. The charge state is determined by whether electrons are exchanged between AB and the electron reservoir (i.e., the surrounding material). (a) If the Fermi level (E_F) is near the conduction band, then the electron reservoir will be more densely populated with electrons. As a result, the 2 electrons will likely remain localized at the vacancy site, forming the V_B^0 charged defect. (b) If E_F is closer to the valence band, then the electron reservoir will be less densely populated, and the 2 electrons will likely delocalize from the vacancy site and join the electron reservoir. This will consequently form the V_B^{+2} charged defect. The E_F-dependent behavior of the electrons can also be described using molecular orbitals. If E_F is near the conduction band and the 2 electrons are localized at the vacancy site as in (a), then this can be interpreted as the filling of a 2-electron molecular orbital state that exists below E_F in energy, denoted "MO". If E_F is near the valence band and the 2 electrons are delocalized from the vacancy site as in (b), then this can be interpreted as depleting the 2-electron MO state.

[a]*Northwestern University, Evanston, IL 60208.*
[*]*E-mail: MichaelToriyama2024@u.northwestern.edu, jeff.snyder@northwestern.edu*

is less likely to proceed with increasing product concentration by Le Chatelier's Principle. Similarly, if the electron reservoir is less populated with electrons when E_F is close to the valence band, then the remaining 2 electrons will likely delocalize from the vacancy site (Figure 1b).

The charge state of a defect can also be understood using the same ideas of chemical bonding and molecular orbital theory that are widely recognized in molecules, as if the charged defect is an atom in a molecule with an associated formal charge. In AB, by removing a B atom from the crystal structure, the surrounding atoms interact and form new molecular orbital states. If E_F is near the conduction band and the 2 electrons remain localized at the defect site, then this can be understood as the filling of a 2-electron molecular orbital state that exists below E_F (Figure 1a). On the other hand, if E_F is close to the valence band and the 2 electrons are delocalized from the defect site, than this can be interpreted as an unfilled molecular orbital state that exists above E_F (Figure 1b).

The consistency between the Le Chatelier's Principle-like perspective and the molecular orbital theory interpretation of charged point defects highlights the simple chemical framework from which we can explain the electronic structures of defects in materials. However, it is not always obvious how such defect-induced molecular orbital states are created, nor where in the electronic structure they form. Here, we use symmetry principles and Density Functional Theory (DFT) calculations to guide a chemical interpretation of charged point defects in materials. We derive chemical interpretations of each native defect in Mg_2Si to demonstrate the simple framework from which we can explain the charge states of point defects. We anticipate that the framework will provide a valuable chemical intuition for defect-induced electronic states that critically affect properties of semiconductor devices, such as photoluminescence, generation/recombination, and electrical transport.

2 Molecular Orbital Diagrams of Point Defects in Mg_2Si

2.1 Crystallography

The charge states of native defects in Mg_2Si can be understood from interactions between the defect atom and the host atoms. Just as in molecules, nearest-neighbor interactions often describe the dominant chemical interactions that lead to molecular orbital states. Accordingly, one must understand the symmetries of each site for which a point defect may reside, and we therefore begin with a discussion of the crystal structure of Mg_2Si.

Mg_2Si crystallizes in the antifluorite structure (Space Group #225, $Fm\bar{3}m$) as shown in Figure 2. Mg occupies all of the tetrahedral sites of the face-centered cubic Si sublattice. Consequently, defects that occupy the Mg site will be tetrahedrally coordinated to 4 neighboring Si atoms (Figure 2b). On the other hand, defects that reside on the Si site will be cubically coordinated[13] to 8 neighboring Mg atoms (Figure 2c). We also consider an interstitial site that is also cubically coordinated to 8 Mg atoms (Figure 2d).

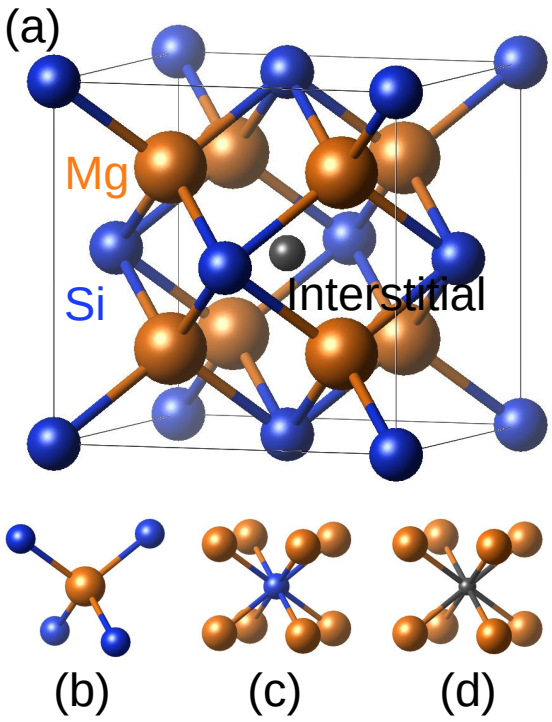

Fig. 2 Antifluorite crystal structure of Mg_2Si (a). Si forms a face-centered cubic sublattice, and Mg fills the tetrahedral sites of the Si sublattice. Accordingly, Mg is tetrahedrally-coordinated by 4 neighboring Si atoms (b), and Si is cubically-coordinated by 8 neighboring Mg atoms (c). The interstitial site considered in this study is also cubically-coordinated by 8 Mg atoms (d).

2.2 Defects Occupying the Interstitial Site

As shown in Figure 2d, a point defect that occupies the interstitial site is cubically coordinated to 8 Mg atoms (Mg_8 for brevity). As a result, we would expect the atomic orbitals of the interstitial atom to interact primarily with the molecular orbitals of the Mg_8 complex, and we therefore begin by drawing the Mg_8 molecular orbitals as one would expect from symmetry. The Mg_8 molecular orbitals near the conduction band edge are primarily constructed from the s-orbitals of the 8 Mg atoms. As shown in Figure 3, the Mg_8 states are split by symmetry into a singlet a_{1g} state, triplet t_{1u} states, triplet t_{2g} states, and a singlet a_{2u} state, labeled according to the O_h point group of the Mg_8 complex.[14,15] The molecular orbitals of the Mg_8 complex are determined using symmetry-adapted linear combinations of atomic orbitals.[16]

Certain interactions between the interstitial atom and the Mg_8 states are allowed by symmetry. For example, we notice in Figure 3a that the singlet a_{1g} state is composed of Mg-s orbitals that are all in phase, indicating that the a_{1g} state is spherically-symmetric. Accordingly, the a_{1g} state can only interact with orbitals of an interstitial atom that are also spherically-symmetric, e.g., an s-orbital. The triplet t_{1u} states all share a feature where the Mg-s orbitals are in phase on the sides of the Mg_8 cube, but out of phase between opposing faces. The t_{1u} states therefore only interact with the p-orbitals of an interstitial atom.

This initial symmetry analysis of the molecular orbitals of the

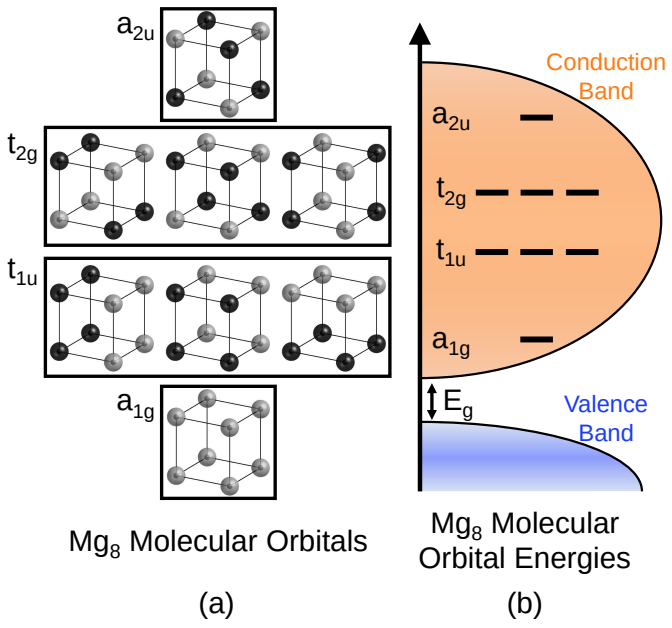

Fig. 3 Molecular orbitals of the Mg_8 complex. The molecular orbitals are composed of Mg-s atomic orbitals, located at the corners of the cubic complex, that split into two singlet states (a_{1g} and a_{2u}) and two sets of triplet states (t_{1u} and t_{2g}) (a). The color of the s-orbital represents the phase. The molecular orbital energies are in the conduction band of Mg_2Si (b), since the conduction band is mainly Mg-s character.

Mg_8 complex guides our understanding of the allowed chemical interactions between an interstitial defect atom and the host atoms near the interstitial site (Figure 4). For example, the s-orbital of the Mg interstitial (Mg_i) interacts with the a_{1g} state of the Mg_8 complex and forms bonding and antibonding states (labeled a_{1g} and a^*_{1g} respectively in Figure 4b), just as in molecules when two atoms form a bond. Similarly, the p-orbitals of Mg_i interact with the triplet t_{1u} states of Mg_8, forming the bonding t_{1u} and antibonding t^*_{1u} states. The t_{2g} and a_{2u} states of Mg_8 however do not interact with any atomic orbital of Mg_i due to symmetry restrictions. A similar analysis can be carried out for the Si interstitial (Si_i), where the s- and p-orbitals of Si_i interact with the a_{1g} and t_{1u} states of Mg_8, respectively (Figure 4e). However, since the energies of the Si atomic orbitals are lower than those of Mg, we would expect the molecular orbital energies of Si_i to be lower than those of Mg_i.

The molecular orbitals resulting from interactions between an interstitial defect atom and the surrounding Mg_8 complex are shown in Figure 5. The bonding a_{1g} state exhibits an in-phase interaction between the s-orbital of the defect atom and the a_{1g} state of the Mg_8 complex, whereas the antibonding a^*_{1g} state consists of an out-of-phase interaction. Similarly, the bonding t_{1u} state is composed of in-phase interactions between the p-orbitals of the interstitial defect atom and the t_{1u} state of the Mg_8 complex, whereas the antibonding t^*_{1u} state exhibits out-of-phase interactions between the p-orbitals and the t_{1u} state of Mg_8. As the t_{2g} and a_{2u} states of the Mg_8 complex do not interact with the s- and p-orbitals of the interstitial defect atom, we do not expect any orbital contribution from the defect atom to those states.

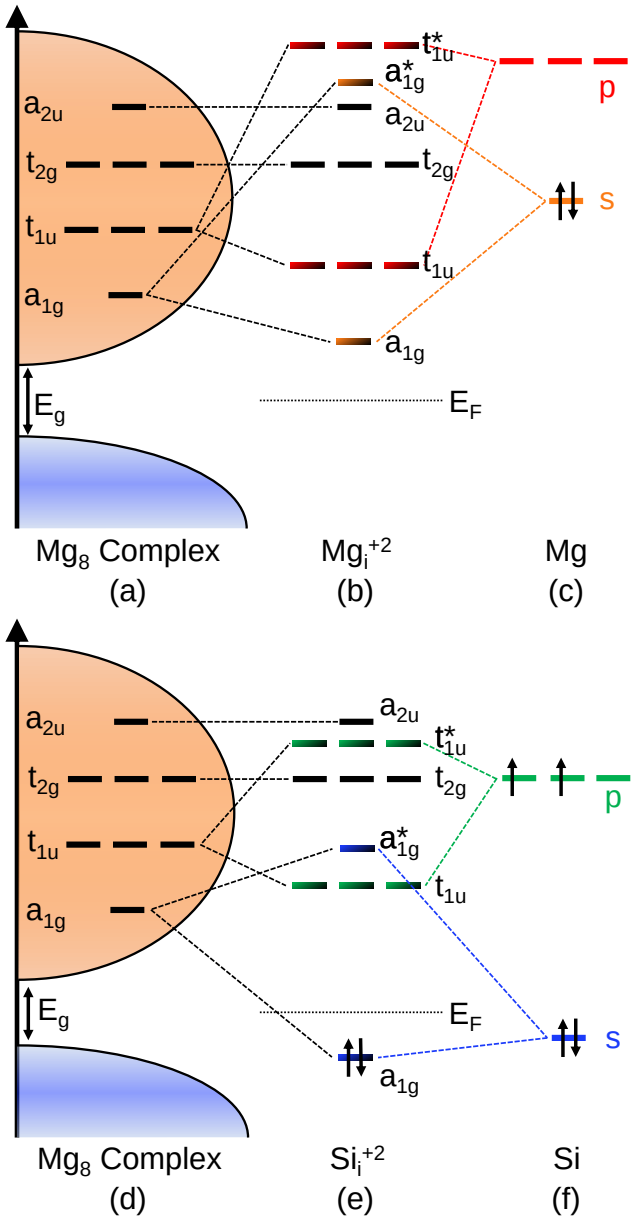

Fig. 4 Molecular orbital diagrams of the Mg interstitial (Mg_i^{+2}), and the Si interstitial (Si_i^{+2}), both of which are 2 electron donors. For Mg_i, the spherically-symmetric a_{1g} state of the Mg_8 complex (a) hybridizes with the s-orbital of the interstitial atom (c), forming the bonding a_{1g} and antibonding a^*_{1g} states (b). The +2 charge state of Mg_i suggests that the bonding a_{1g} state is located in the conduction band (b), such that the state is depopulated by 2 electrons when E_F is in the band gap. Similarly, for Si_i, the a_{1g} state of the Mg_8 complex (d) hybridizes with the s-orbital of Si (f) to form the bonding a_{1g} and antibonding a^*_{1g} states (e), and the t_{1u} states of Mg_8 (d) interact with the p-orbitals of Si (f) to form the bonding t_{1u} and antibonding t^*_{1u} states (e). If the bonding t_{1u} state exists in the conduction band and the bonding a_{1g} state resides in the valence band, then Si_i has a +2 charge state due to the removal of 2 electrons from the bonding t_{1u} state when E_F is in the band gap.

While the molecular orbital energies of Mg_i and Si_i in relation to the conduction and valence bands of Mg_2Si (Figures 4b, 4e) are certainly unclear from this analysis, symmetry provides valuable insight towards the degeneracies of the molecular orbitals and

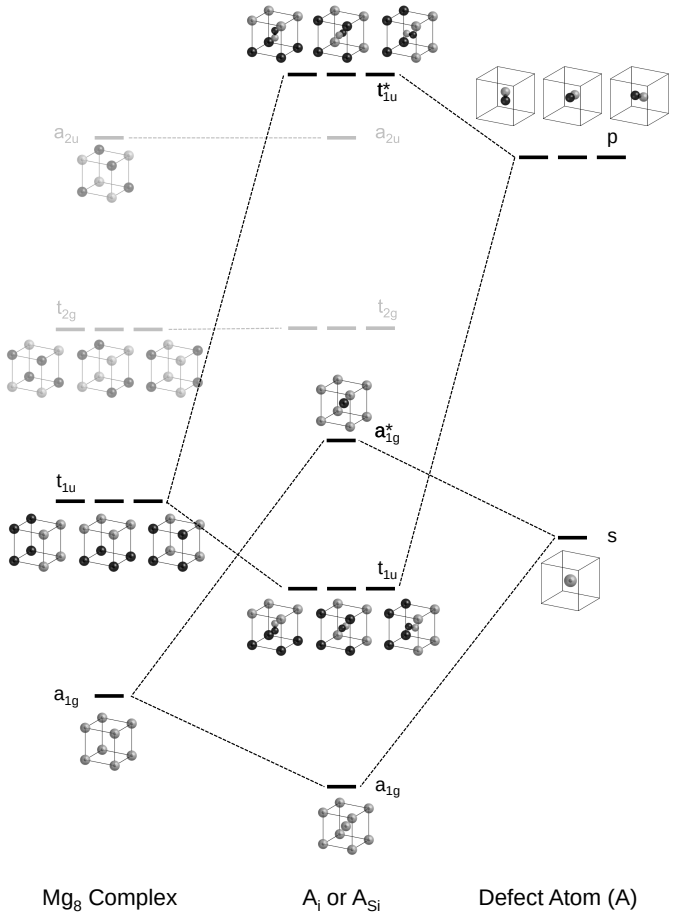

Fig. 5 The molecular orbitals resulting from interactions between the Mg_8 complex and the s- and p-orbitals of a defect atom A occupying either an interstitial site (A_i) or an Si site (A_{Si}) in Mg_2Si. The shading of each s- and p-orbital represents the relative phase of the orbital.

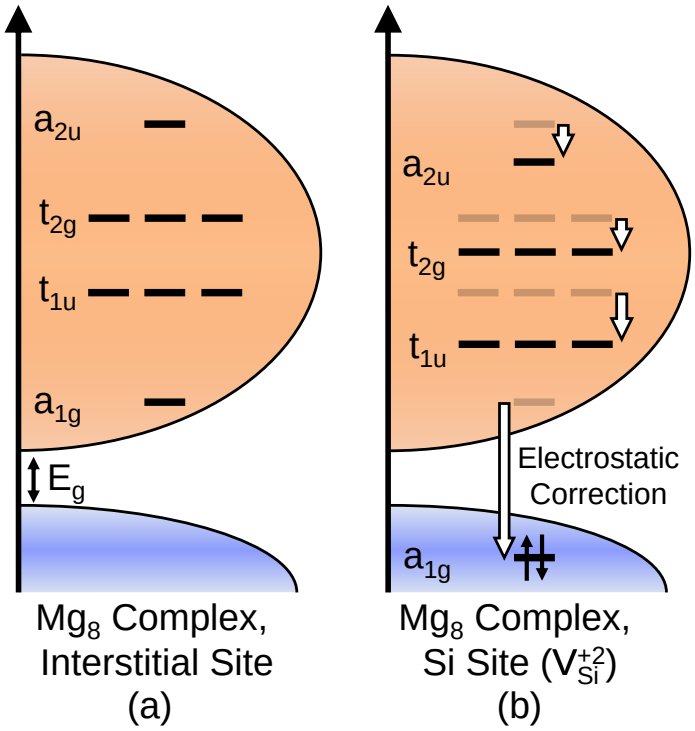

Fig. 6 Molecular orbital diagram of the Si vacancy (V_{Si}^{+2}), which is a 2 electron donor. The energies of the Mg_8 molecular orbitals surrounding a Si vacancy (b), which are the molecular orbitals of V_{Si}, are lower than those surrounding an empty interstitial site (a), due to electrostatic corrections arising from the attractive Madelung potential of an anionic vacancy site.

the possible charge states of the defects. For Mg_i^0, the bonding a_{1g} state is filled with 2 electrons, due to the 2 valence electrons introduced by the interstitial Mg atom. As we will see in Section 3.2, DFT calculations indicate that Mg_i has a +2 charge state when E_F is in the band gap. This suggests that the bonding a_{1g} state is located in the conduction band (Figure 4b) such that the 2 electrons are delocalized from the Mg_i defect when E_F is in the band gap. For Si_i^0, the bonding a_{1g} and t_{1u} states are both filled with 2 electrons each, as the interstitial Si atom introduces four valence electrons. DFT calculations indicate that Si_i has a +2 charge state when E_F is in the band gap (Section 3.2). A chemical interpretation consistent with this observation is that the bonding a_{1g} state is located in the valence band while the bonding t_{1u} state is in the conduction band, such that the Si_i^{+2} charged defect forms from the delocalization of 2 electrons from the t_{1u} state (Figure 4e).

2.3 Defects Occupying the Si Site

A defect that occupies the Si site in Mg_2Si is cubically coordinated to 8 Mg atoms (Figure 2c), similar to the interstitial case. As a result, the defect will interact with the same Mg_8 molecular orbitals that we consider for the interstitial site.

We begin with a discussion of the Si vacancy (V_{Si}), since the electronic structure of this defect can be understood solely from the Mg_8 molecular orbitals. While the molecular orbitals themselves are the same as those surrounding the interstitial site (Figure 3a), their energies will be lower due to the attractive Madelung potential of the anionic vacancy site[17] (Figure 6). Additionally, while the molecular orbitals of the Mg_8 complex surrounding the interstitial site are unfilled, the molecular orbitals surrounding the vacant Si site are filled with 4 electrons, which fill the bottom singlet a_{1g} state with 2 electrons and the triplet t_{1u} states with 2 electrons. DFT calculations suggest that the charge state of V_{Si} is primarily +2 when E_F is in the band gap (Section 3.2). A consistent molecular orbital theory-based interpretation of V_{Si}^{+2} is that the a_{1g} state is located in the valence band and the t_{1u} states are located in the conduction band, which results in the depopulation of the t_{1u} states by 2 electrons when E_F is in the band gap (Figure 6b). Note that this description is also consistent with the lowering of the molecular orbital energies by the Madelung potential.

The atomic orbitals of the Mg on Si antisite defect (Mg_{Si}) interact with the Mg_8 molecular orbitals surrounding the Si site, for which the energies are the same as those for V_{Si} (Figures 6b, 7a). Since a Mg atom occupies a Si site in Mg_{Si}, the atomic orbital energies of the Mg atom will be shifted downwards due to the Madelung potential, which is attractive for electrons at an an-

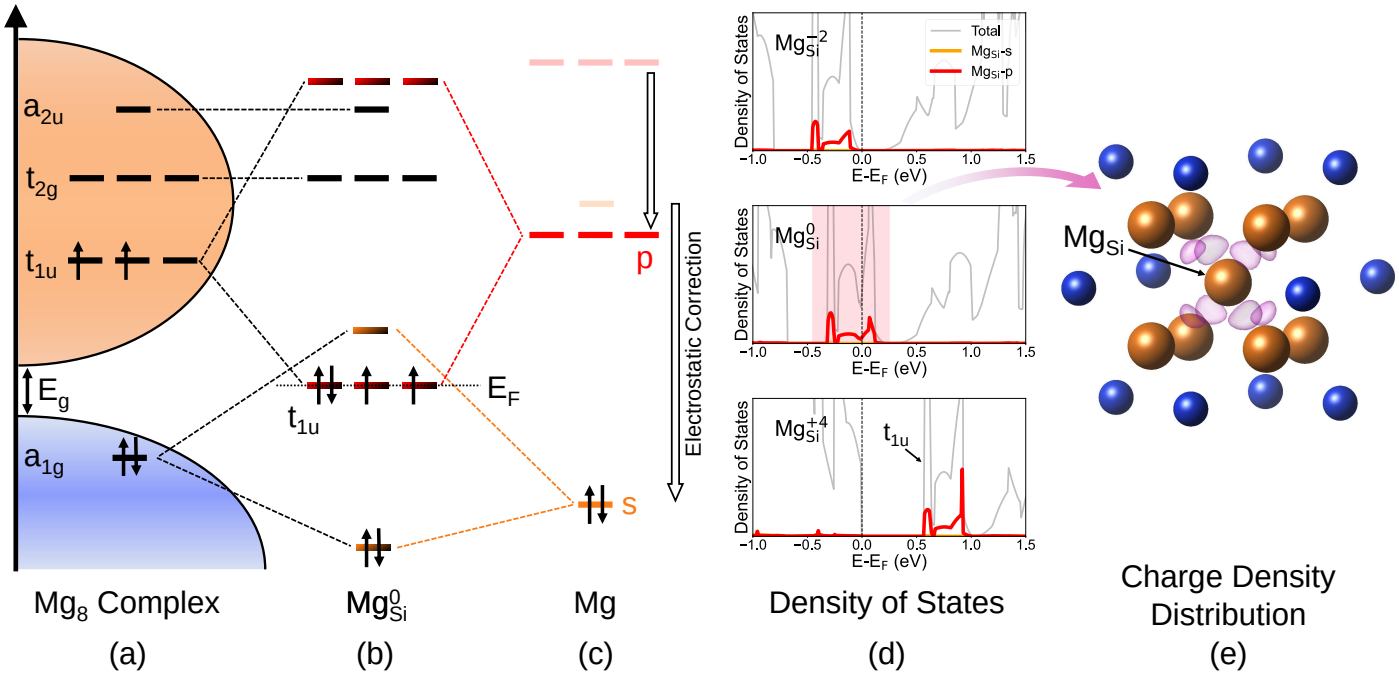

Fig. 7 Molecular orbital diagram for the Mg on Si antisite defect (Mg_{Si}). The molecular orbitals of the Mg_8 complex surrounding a vacant Si site (Figure 6b) (a) will interact with the atomic orbitals of the Mg atom occupying the Si site (c). The atomic orbitals of Mg are pushed down in energy by the electrostatic Madelung potential, since the Mg atom is occupying an anionic Si site which is attractive for electrons. Interactions between the molecular orbitals of Mg_8 and the atomic orbitals of the Mg atom results in a partially-filled set of bonding t_{1u} states for the Mg^0_{Si} defect (b). The density of states of Mg_2Si, with a Mg_{Si} defect included, exhibits a set of peaks which is partially Mg_{Si}-p character (d). These peaks correspond to the bonding t_{1u} states, since the peaks can hold up to 6 electrons total as they are completely filled when 2 electrons are added to the system (Mg^{-2}_{Si}) and empty when 4 electrons are taken away (Mg^{+4}_{Si}). The charge density distribution, which is calculated from states within the highlighted energy window for Mg^0_{Si}, shows that the bonding t_{1u} states are localized at the Mg_{Si} defect site (e).

ion site (Figure 7c).[17] The s- and p-orbitals of the Mg atom will interact with the a_{1g} and t_{1u} states of Mg_8, respectively, forming the same molecular orbitals as those for an interstitial defect (Figure 5). Since there are 4 electrons from the Mg_8 complex and 2 valence electrons from the Mg atom, there are 6 electrons that fill the molecular orbitals of Mg^0_{Si}, which results in partially-filled bonding t_{1u} states (Figure 7b).

The charge state of Mg_{Si} ranges from +4 when E_F is near the valence band to -2 when E_F is near the conduction band (Section 3.2). This suggests that the partially-filled bonding t_{1u} states are located in the band gap of Mg_2Si, so that the states are deprived of 4 electrons when E_F is close to the valence band edge and supplied with 2 electrons when E_F is near the conduction band edge. As evidenced by the DFT-calculated partial density of states (Figure 7d), peaks that are primarily composed of p-orbitals of the Mg_{Si} defect atom exist in the electronic structure. These peaks correspond to the bonding t_{1u} states; the peaks are completely filled when 2 additional electrons are added (Mg^{-2}_{Si}) and empty when 4 electrons are taken away (Mg^{+4}_{Si}), indicating that the peaks can hold up to 6 electrons just like the bonding t_{1u} states. The charge density distributions of the bonding t_{1u} states (Figure 7e) are mostly localized to the Mg_{Si} defect atom as opposed to being spread over the host atoms, indicating that the bonding t_{1u} states do not mix with the conduction/valence band states and are therefore localized states in the band gap.

2.4 Defects Occupying the Mg Site

Defects that occupy the Mg site in Mg_2Si are tetrahedrally coordinated to 4 Si atoms (Figure 2b), which we refer to collectively as the "Si_4 complex" for brevity. The electronic structure of the Mg vacancy (V_{Mg}) can be understood from the molecular orbitals of the Si_4 complex. The energies of the molecular orbitals constructed from the Si-p states are split into a singlet a_1 state, two sets of triplet t_2 states, doublet e states, and triplet t_1 states (Figure 8). The molecular orbitals are determined using symmetry-adapted linear combinations of atomic orbitals[16] and labeled by symmetry according to the T_d point group of the Si_4 complex (derivation shown in the Supplementary Information).[14,15]

Normally in the Mg_2Si solid, there are two Mg cations that donate 2 valence electrons each to one Si anion, so that each ion has a closed shell electron configuration. The Si_4 molecular orbitals are similarly filled by valence electrons from 8 Mg atoms in a perfect, undefected crystal. However, by removing a Mg atom to create the V_{Mg} defect, the number of electrons filling the Si_4 states changes. In total there are (2 p-orbital valence electrons per Si) $\times$ (4 Si atoms) + (2 s-orbital valence electrons per Mg) $\times$ (7 Mg atoms) = 22 electrons that fill the Si_4 states, which would leave the high-energy t_2 states deficient of 2 electrons. When E_F is in the band gap, V_{Mg} has a -2 charge state (Section 3.2). It is therefore reasonable to interpret the -2 charge state as a filling of the t_2 states by 2 additional electrons from the electron reservoir, forming the V^{-2}_{Mg} charged defect (Figure 8b).

The Si on Mg antisite defect (Si_{Mg}) interacts primarily with Si_4 as it occupies the Mg site, and we can therefore understand the electronic structure of the defect through interactions between the atomic orbitals of the Si defect atom and the molecular orbitals of Si_4 (Figure 9). Analogous to the Mg_{Si} defect, the Madelung potential raises the atomic orbital energies of the Si atom (Figure 9c), since a cation site is repulsive for electrons.[17] By symmetry, the s-orbital of the Si defect atom will only interact with the spherically-symmetric a_1 state of Si_4, and the p-orbitals of the Si defect atom will only interact with the t_2 states of Si_4. The 26 total electrons from Si_4 (22 electrons) and the Si defect atom (4 electrons) will completely fill the molecular orbitals of Si_{Mg} up to and including the antibonding a_1^* state (Figure 9b).

It turns out that the a_1^* state is a localized state residing in the band gap of Mg_2Si. DFT calculations indicate that the charge state of Si_{Mg} is +2 when E_F is near the valence band and 0 when E_F is near the conduction band (Section 3.2). A chemical explanation for this charge state transition is that the antibonding a_1^* state is in the band gap, such that the charge state is neutral when E_F is above the a_1^* state (as in Figure 9b) and 2 electrons are depopulated from the a_1^* state when E_F is near the valence band edge. The partial density of states of Si_{Mg} in Mg_2Si corroborates this interpretation, where a 2 electron state that is predominantly s-character is filled in Si^0_{Mg} and empty in Si^{+2}_{Mg} (Figure 9d). Moreover, the charge density of the a_1^* state is primarily centered around the Si_{Mg} defect site (Figure 9e) as opposed to being spread

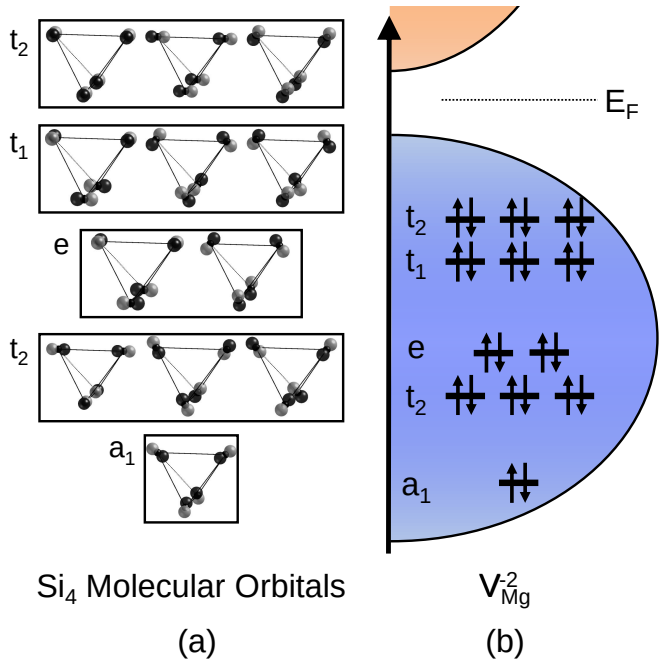

Fig. 8 Molecular orbital diagram of the Mg vacancy (V^{-2}_{Mg}), which is a 2 electron acceptor. The molecular orbitals of the Si_4 complex surrounding a Mg site are composed of p-orbitals of the 4 Si atoms. The p-orbitals hybridize and split into an s-like a_1 state, two sets of p-like t_2 triplets, an e doublet, and a t_1 triplet (a). The shading represents the relative phases of the orbitals. The molecular orbital energies are in the valence band of Mg_2Si (b). There are 22 electrons total when V_{Mg} is created, which fill the molecular orbitals up to the t_1 state and partially fills the top t_2 state with 4 electrons. The -2 charge state of V_{Mg} suggests that the t_2 states exist in the valence band, so that 2 additional electrons completely fill the t_2 states when E_F is in the band gap. Rotating depictions of the Si_4 molecular orbitals are available as GIFs in a public repository.[18]

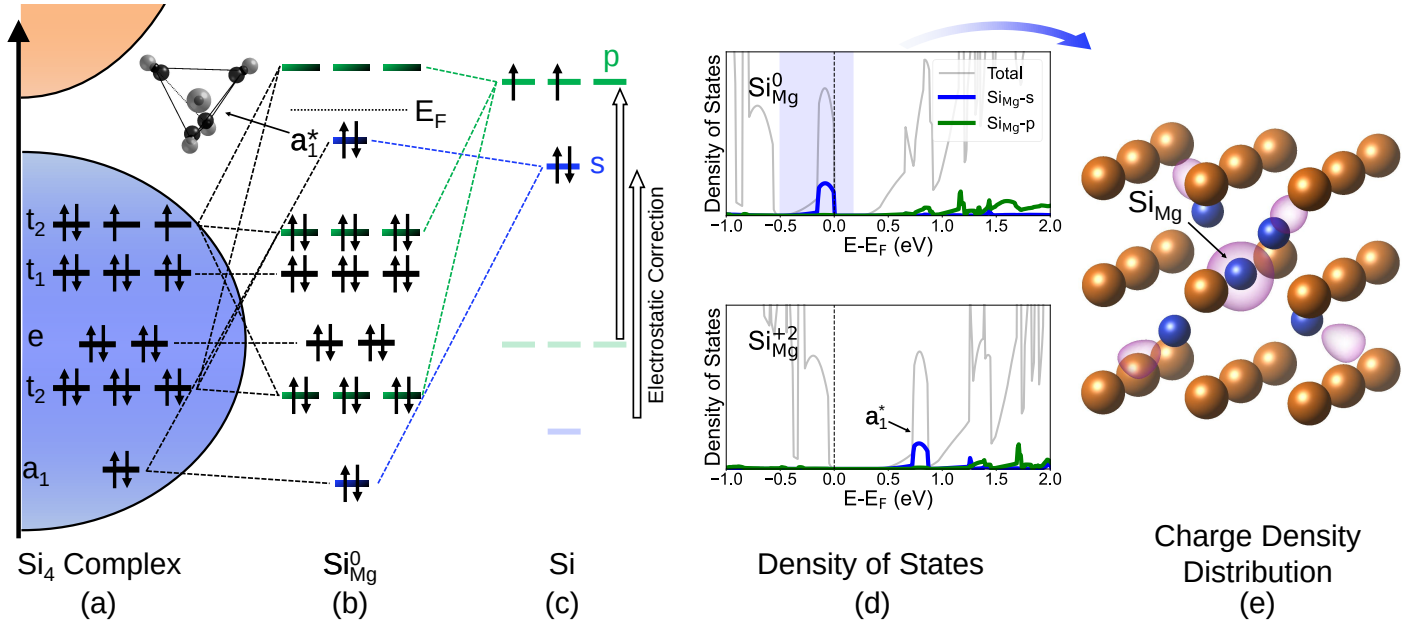

Fig. 9 Molecular orbital diagram of the Si on Mg antisite defect (Si_{Mg}). The atomic orbitals of the Si atom (c) are raised in energy due to the electrostatic Madelung potential from occupying the cationic Mg site, which is repulsive for electrons. The atomic orbitals of the Si atom will hybridize with the molecular orbitals of the Si_4 complex (a) to form the molecular orbitals of the Si_{Mg} defect (b); in particular, the spherically-symmetric a_1 state of the Si_4 complex will interact with the s-orbital of the Si atom, forming the antibonding a_1^* state in the band gap. The molecular orbital of the a_1^* state as expected from molecular orbital theory is drawn, where the shading of each orbital represents the relative phase. The partial density of states of the Si_{Mg} defect atom (d) exhibits a 2-electron state which is composed primarily of the s-orbital. The charge density of the states within the highlighted portion (e) shows that the charge is localized at the Si_{Mg} defect atom, and the nodal structure (i.e., absence of charge between Si_{Mg} and the surrounding Si atoms) indicates antibonding character. Therefore, the 2-electron state in (d) corresponds to the antibonding a_1^* state in (b).

over regions far from the defect, indicating that the a_1^* state is a localized state that does not mix with either the conduction nor valence band states.

The nodal feature of the charge density, in which there is no charge between the central Si defect atom and the surrounding Si_4 complex (Figure 9e), indicates antibonding character consistent with the description of the a_1^* state. In fact, the charge density calculated using DFT agrees with our molecular orbital theory analysis. As drawn in Figure 9b, we expect from molecular orbital theory that the a_1^* state consists of a spherical s-orbital at the center of the tetrahedral complex that is out-of-phase with the a_1 state of the Si_4 complex (Figure 8a). Since the orbitals (i.e., wave functions) are out-of-phase, we expect destructive interference between the s-orbital and the a_1 state of Si_4. As a result, the wave function should be zero in the region between the defect atom and the vertices of the Si_4 complex, in agreement with the charge density profile shown in Figure 9e.

3 Connection to Defect Formation Energies

3.1 General Overview of Defect Formation Energies

The charge states of point defects are oftentimes understood from the formation energies of defects, provided that the dependence on E_F is addressed.[2] When the charged defect V_B^{+2} is formed in a hypothetical II-VI semiconductor AB, exchanges between the crystal and both an atomic reservoir *and* an electron reservoir take place, summarized by the equation

$$(\text{Perfect AB}) \rightarrow (\text{AB with } V_B^{+2}) + B + 2e^-. \quad (1)$$

Each term in this "defect reaction" is associated with an energy from which the formation energy of V_B^{+2} is derived:

$$\Delta H_{V_B^{+2}} = \left(E_{V_B^{+2}} + \mu_B + 2E_F\right) - E_{\text{Perfect}} \quad (2)$$

where $E_{V_B^{+2}}$ and E_{Perfect} are the energies of AB with and without V_B^{+2}, respectively, μ_B is the atomic chemical potential of atom B, and E_F is the electron chemical potential (i.e., the Fermi level). Notice that the formation energy of V_B^{+2} depends on E_F, since 2 electrons leave the vacancy site as "reaction products". This is not true for the neutral charge V_B^0 defect, where no relative change in the number of electrons occurs. Consequently, the formation energy of V_B^0 is independent of E_F:

$$\Delta H_{V_B^0} = \left(E_{V_B^0} + \mu_B\right) - E_{\text{Perfect}} \quad (3)$$

where $E_{V_B^0}$ is the energy of AB with the V_B^0 defect. In general, the formation energy of any charged point defect (i.e., vacancies, interstitials, antisites, and substitutionals) can be deduced from a "defect reaction equation" and therefore has the general form:[2,7]

$$\Delta H_{D^q} = E_{D^q} - E_{\text{Perfect}} - \sum n_i \mu_i + qE_F \quad (4)$$

for a defect D with charge state q, where the sum runs over all atomic species i involved in creating the point defect, and n_i is the number of atoms added ($n_i > 0$) or removed ($n_i < 0$) to create

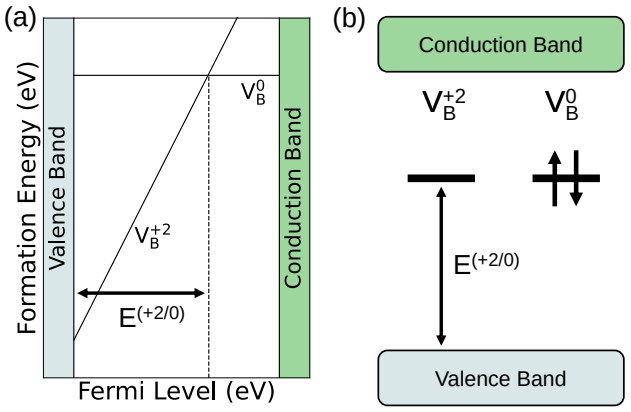

Fig. 10 The defect formation energy diagram of the B vacancy V_B in a hypothetical II-VI compound AB (a). The slope of the formation energy of the vacancy changes at $E^{(+2/0)}$ above the valence band maximum, which corresponds to a transition between the vacancy releasing 2 electrons to the electron reservoir (V_B^{+2}) and the vacancy retaining the 2 electrons (V_B^0). This change in behavior can correspondingly be interpreted as populating or depopulating a molecular orbital at $E^{(+2/0)}$ above the valence band maximum (b), where an unfilled molecular orbital corresponds to V_B^{+2} and a filled orbital corresponds to V_B^0.

the defect.

The charge states of defects can be understood diagrammatically by treating E_F as a variable, plotting the formation energies of a defect in different charge states, and identifying the charge state with the lowest formation energy at each E_F. As shown schematically in Figure 10a, the formation energy of V_B^{+2} is lower than that of V_B^0 when E_F is close to the valence band maximum (note that the slope of the formation energy corresponds to the charge state by Equation 4), indicating that V_B^{+2} is more likely to form than V_B^0 when AB is *p*-type. The opposite is true when E_F is closer to the conduction band minimum, where the formation energy of V_B^0 is lower than that of V_B^{+2}.

For illustrative purposes, we show that the formation energies of V_B^{+2} and V_B^0 cross at $E_F = E^{(+2/0)}$, signifying a transition in the charge state of V_B. A chemical interpretation consistent with this charge state transition is that a molecular orbital, which is induced by the defect, exists with energy $E^{(+2/0)}$ above the valence band maximum. The molecular orbital is unfilled when E_F is below in energy (forming the V_B^{+2} charged defect) and filled when E_F is above in energy (creating the V_B^0 defect), as shown in Figure 10b. Note that this charge transition need not occur in the band gap, as the molecular orbital(s) induced by the defect may appear inside the bands instead.

3.2 Formation Energies of Defects in Mg_2Si

The formation energies of all charged native defects of Mg_2Si, which are calculated using DFT, are shown in Figure 11, in agreement with previous studies.[19,20] Some native defects have a single charge state corresponding to having all filled or unfilled molecular orbitals in the valence or conduction bands, while others have multiple charge states corresponding to the existence of a molecular orbital state in the band gap.

For Mg_i, the +2 charge state corresponds to the depopulation

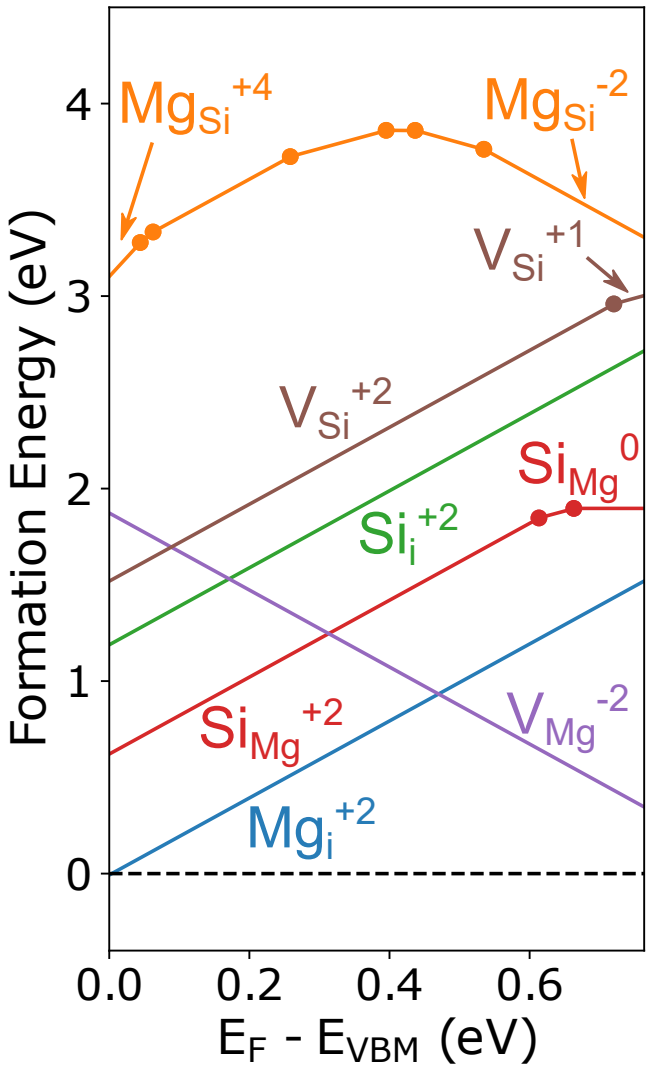

Fig. 11 Formation energies of native defects in Mg_2Si, shown for Si-rich conditions. The defect formation energy is plotted against the Fermi level E_F, referenced to the valence band maximum (E_{VBM}), and is plotted from the valence band maximum to the conduction band minimum.

of the bonding a_{1g} molecular orbital (Figure 4b), which exists in the conduction band so that Mg_i^{+2} forms when E_F is in the band gap. The +2 charge state of Si_i suggests that the fully-occupied singlet bonding a_{1g} state is in the valence band and the partially-occupied triplet bonding t_{1u} states are in the conduction band (Figure 4e), such that the charge state can be interpreted as a depopulation of the t_{1u} states by 2 electrons.

The -2 charge state of V_{Mg} corresponds to the filling of the t_2 state of the Si_4 molecular orbitals with 2 additional electrons (Figure 8b), which exist in the valence band so that V_{Mg}^{-2} forms when E_F is in the band gap. Similarly, the mainly +2 charge state of V_{Si} corresponds to the depopulation of the t_{1u} states of the Mg_8 complex (Figure 6b), which in the neutral charge state is filled with 2 electrons.

Both antisite defects exhibit charge state transitions within the band gap, which correspond to the existence of molecular orbitals

in the band gap. The transition from Si_{Mg}^{+2} near the valence band maximum to Si_{Mg}^{0} near the conduction band minimum (i.e., a difference of 2 in the charge state) corresponds to populating the 2-electron antibonding a_1^* state residing in the band gap (Figure 9b). If E_F is above the a_1^* state, then the state is filled and the Si_{Mg} antisite defect has a neutral charge state; on the other hand, if E_F is below the a_1^* state, then the state is unfilled and the Si_{Mg}^{+2} charged defect forms. The transition in the charge state of the Mg_{Si} antisite defect from +4 near the valence band maximum to -2 near the conduction band minimum (i.e., a difference of 6 in the charge state) is also explained by a filling of the 6-electron bonding t_{1u} states (Figure 7b). If E_F is below the t_{1u} states, then the states are completely empty and devoid of 4 electrons, corresponding to the Mg_{Si}^{+4} charged defect; on the other hand, if E_F is above the t_{1u} states and near the conduction band minimum, then the states are completely filled and has 2 additional electrons, corresponding to the Mg_{Si}^{-2} charged defect.

4 Discussion

The defect formation energy diagram (Figure 11) and bonding symmetry are used to guide a chemical understanding of point defects in Mg_2Si. This *interpretive* chemical understanding of defects allows us to understand which molecular orbitals are populated/depopulated resulting in the charge state(s) of a defect. While secondary effects such as next-nearest neighbor interactions[21] and lattice distortions[4,22–24] play a role, the present analysis suggests that local interactions between a defect atom and the surrounding host atoms (or, in the case of the vacancies, interactions amongst the host atoms surrounding the vacancy site) provide a sufficient explanation for the defect charge states in the defect formation energy diagram. It is worth noting however that the relative energy placement of the molecular orbital with respect to the band edges is contingent on the accuracy of the DFT-calculated defect formation energy diagram; for example, had the charge state of V_{Si} been +4 instead of +2, we would interpret the chemistry of the defect as involving the depopulation of both the t_{1u} states and the a_{1g} state, which would imply that the a_{1g} state resides in the conduction band instead of the valence band (Figure 6b).

Molecular orbitals have been used to quantitatively describe defects in several specific examples[25–28] including native defects in silicon,[29] the anion vacancy in binary II-VI compounds,[22,30] substitutional defects in III-V compounds,[31] and recently in qubit technologies.[32,33]

Yet, the qualitative framework described here can be used more generally to understand the charge states of defects and explain chemical trends. This can be a valuable guide for applications in which doping is essential for tuning the electrical properties of materials, such as thermoelectrics[34–36] and transparent conducting oxides.[37–40] In fact, the present molecular orbital analyses for Mg_2Si can directly be applied to compounds with structures having the same atomic positions, such as half-Heusler TiNiSn[41,42] and fluorite CeO_2.[43]

5 Conclusion

We discuss a chemical interpretation of the charge states of point defects in materials. Notably, we use molecular orbital theory and symmetry principles to guide our understanding of the charge state(s) of a defect, as the framework qualitatively captures the local defect-host interactions leading to molecular orbital states in the electronic structure. The chemical interactions between the defect atom and host atoms can be understood from symmetry principles, as some interactions are forbidden. While the present analysis neglects second-order effects such as lattice distortions and next-nearest neighbor interactions, many of the charge states appearing in the formation energies of native defects in Mg_2Si are understood qualitatively from the molecular orbital theory framework.

Methods

All first-principles Density Functional Theory (DFT) calculations were performed used the Vienna ab-initio simulation package (VASP)[44–46] using the projector-augmented wave (PAW) method[47,48] and an energy cutoff of 500 eV. The Mg and Si pseudopotentials, which explicitly treat the $3s^2$ and $3s^23p^2$ valence electrons respectively, were used.

A 2x2x2 supercell of the 12-atom cubic structure (96 atoms total) of Mg_2Si was generated to perform defect calculations. Ionic relaxations were performed with a force convergence criterion of 0.02 eV/Å and a Γ-centered[49] k-point mesh density of 2x2x2 was used for all point defect calculations. A static calculation using the tetrahedron method with Blöchl corrections[50] with an increased k-point mesh density of 3x3x3 was performed on the relaxed structures to produce accurate total energies and density of states.

It is well known that the self-interaction error inherent to DFT causes uncertainty in the absolute energies of the Kohn-Sham states.[2,23,24] Since the single particle states are crucial for this study when reconciling defect charge transitions and the density of states, all point defect calculations employed the hybrid HSE06 functional.[51–53] We set the exact exchange mixing parameter to 0.37, which yielded an indirect band gap of 0.76 eV in agreement with the experimentally measured band gap of 0.78 eV.[54] The defect formation energy ΔH_{D^q} of a defect D with charge state q is calculated using the equation

$$\Delta H_{D^q} = E_{D^q} - E_{\text{Perfect}} - \sum n_i \mu_i + qE_F + E_{\text{Corr}} \qquad (5)$$

where the first four terms on the right hand side of the equation are explained in the main text. The last term, E_{Corr}, accounts for correction terms arising from finite-size effects.[2,55] The chemical potential, $\mu_i = \mu_i^\circ + \Delta\mu_i$, can be expressed as a deviation from the reference elemental chemical potential. We set $\Delta\mu_{Mg} = \frac{1}{2}\Delta H_{Mg_2Si}$ and $\Delta\mu_{Si} = 0$ for the Si-rich defect formation energy diagram, where ΔH_{Mg_2Si} is the formation enthalpy of Mg_2Si.

Acknowledgements

M.Y.T. is funded by the United States Department of Energy through the Computational Science Graduate Fellowship (DOE CSGF) under grant number DE-SC0020347. M.K.B. and G.J.S.

acknowledge support from NSF DMREF grant number 1729487. This research was supported in part through the computational resources and staff contributions provided for the Quest high performance computing facility at Northwestern University, which is jointly supported by the Office of the Provost, the Office for Research, and Northwestern University Information Technology.

References

1 F. Kröger and H. Vink, *Solid State Phys.*, 1956, **3**, 307.

2 C. Freysoldt, B. Grabowski, T. Hickel, J. Neugebauer, G. Kresse, A. Janotti and C. G. Van de Walle, *Rev. Mod. Phys.*, 2014, **86**, 253.

3 X. Peng-Shou, S. Yu-Ming, S. Chao-Shu, X. Fa-Qiang and P. Hai-Bin, *Chinese Phys. Lett.*, 2001, **18**, 1252.

4 A. Janotti and C. G. Van de Walle, *Appl. Phys. Lett.*, 2005, **87**, 122102.

5 A. Janotti and C. G. Van de Walle, *J. Cryst. Growth*, 2006, **287**, 58.

6 A. Janotti and C. G. Van de Walle, *Phys. Rev. B*, 2007, **76**, 165202.

7 S. Lany and A. Zunger, *Phys. Rev. B*, 2008, **78**, 235104.

8 A. Janotti and C. G. Van de Walle, *Rep. Prog. Phys.*, 2009, **72**, 126501.

9 S. Clark, J. Robertson, S. Lany and A. Zunger, *Phys. Rev. B*, 2010, **81**, 115311.

10 F. Oba, M. Choi, A. Togo and I. Tanaka, *Sci. Technol. Adv. Mat.*, 2011, **12**, 034302.

11 M. D. McCluskey and S. Jokela, *J. Appl. Phys.*, 2009, **106**, 10.

12 S. Kim, S. N. Hood, J.-S. Park, L. D. Whalley and A. Walsh, *J. Phys. Energy*, 2020, **2**, 036001.

13 D. Luo, J. Lv, F. Peng, Y. Wang, G. Yang, M. Rahm and Y. Ma, *Chem. Sci.*, 2019, **10**, 2543.

14 F. A. Cotton, *Chemical applications of group theory*, John Wiley & Sons, 2003.

15 M. S. Dresselhaus, G. Dresselhaus and A. Jorio, *Group theory: application to the physics of condensed matter*, Springer Science & Business Media, 2007.

16 T. A. Albright, J. K. Burdett and M.-H. Whangbo, *Orbital interactions in chemistry*, John Wiley & Sons, 2013.

17 P. A. Cox, *The electronic structure and chemistry of solids*, Oxford University Press, 1987.

18 https://github.com/mathtoriyama/Papers/tree/main/2021/Mg2Si-Defects.

19 A. Kato, T. Yagi and N. Fukusako, *J. Phys. Condens. Mat.*, 2009, **21**, 205801.

20 B. Ryu, E.-A. Choi, S. Park, J. Chung, J. de Boor, P. Ziolkowski, E. Müller and S. Park, *J. Alloy. Compd.*, 2021, **853**, 157145.

21 J. Neugebauer and C. G. Van de Walle, *Phys. Rev. B*, 1994, **50**, 8067.

22 S. Lany and A. Zunger, *Phys. Rev. B*, 2005, **72**, 035215.

23 S. Lany and A. Zunger, *Phys. Rev. B*, 2009, **80**, 085202.

24 S. Lany, *Phys. Status Solidi B*, 2011, **248**, 1052.

25 A. M. Stoneham, *Theory of defects in solids: electronic structure of defects in insulators and semiconductors*, Oxford University Press, 2001.

26 R. Messmer and G. Watkins, *Phys. Rev. B*, 1973, **7**, 2568.

27 G. D. Watkins, *Physica B + C*, 1983, **117**, 9.

28 A. Janotti and C. G. Van de Walle, *Nat. Mater.*, 2007, **6**, 44.

29 G. D. Watkins, *Phys. Solid State*, 1999, **41**, 746.

30 B. Meyer and W. Stadler, *J. Cryst. Growth*, 1996, **161**, 119.

31 H. P. Hjalmarson, P. Vogl, D. J. Wolford and J. D. Dow, *Phys. Rev. Lett.*, 1980, **44**, 810.

32 J. Weber, W. Koehl, J. Varley, A. Janotti, B. Buckley, C. Van de Walle and D. D. Awschalom, *P. Natl. Acad. Sci.*, 2010, **107**, 8513.

33 I. Harris, C. J. Ciccarino, J. Flick, D. R. Englund and P. Narang, *Phys. Rev. B*, 2020, **102**, 195206.

34 G. J. Snyder and E. S. Toberer, 2008, **7**, 105.

35 Q. Song, J. Zhou, L. Meroueh, D. Broido, Z. Ren and G. Chen, *Appl. Phys. Lett.*, 2016, **109**, 263902.

36 Q. Zhang, Q. Song, X. Wang, J. Sun, Q. Zhu, K. Dahal, X. Lin, F. Cao, J. Zhou, S. Chen, G. Chen, J. Mao and R. Zhifeng, *Energ. Environ. Sci.*, 2018, **11**, 933.

37 K. H. Zhang, K. Xi, M. G. Blamire and R. G. Egdell, *J. Phys. Condens. Mat.*, 2016, **28**, 383002.

38 S. Lany and A. Zunger, *Phys. Rev. Lett.*, 2007, **98**, 045501.

39 D. O. Scanlon, *Phys. Rev. B*, 2013, **87**, 161201.

40 J. L. Lyons, D. Steiauf, A. Janotti and C. G. Van de Walle, *Phys. Rev. Appl.*, 2014, **2**, 064005.

41 W. G. Zeier, J. Schmitt, G. Hautier, U. Aydemir, Z. M. Gibbs, C. Felser and G. J. Snyder, *Nat. Rev. Mater.*, 2016, **1**, 1.

42 S. J. Poon, *Metals*, 2018, **8**, 989.

43 R. Schmitt, A. Nenning, O. Kraynis, R. Korobko, A. I. Frenkel, I. Lubomirsky, S. M. Haile and J. L. Rupp, *Chem. Soc. Rev.*, 2020, **49**, 554.

44 G. Kresse, *J. Non-Cryst. Solids*, 1995, **192**, 222.

45 G. Kresse and J. Furthmüller, *Comp. Mater. Sci.*, 1996, **6**, 15.

46 G. Kresse and J. Furthmüller, *Phys. Rev. B*, 1996, **54**, 11169.

47 P. E. Blöchl, *Phys. Rev. B*, 1994, **50**, 17953.

48 G. Kresse and D. Joubert, *Phys. Rev. B*, 1999, **59**, 1758.

49 H. J. Monkhorst and J. D. Pack, *Phys. Rev. B*, 1976, **13**, 5188.

50 P. E. Blöchl, O. Jepsen and O. K. Andersen, *Phys. Rev. B*, 1994, **49**, 16223.

51 J. Heyd, G. E. Scuseria and M. Ernzerhof, *J. Chem. Phys.*, 2003, **118**, 8207.

52 J. Heyd and G. E. Scuseria, *J. Chem. Phys.*, 2004, **121**, 1187.

53 A. V. Krukau, O. A. Vydrov, A. F. Izmaylov and G. E. Scuseria, *J. Chem. Phys.*, 2006, **125**, 224106.

54 R. G. Morris, R. Redin and G. Danielson, *Phys. Rev.*, 1958, **109**, 1909.

55 C. Freysoldt, J. Neugebauer and C. G. Van de Walle, *Phys. Rev. Lett.*, 2009, **102**, 016402.